Korean J. Chem. Eng., 37(1), 151-158 (2020)
DOI: 10.1007/s11814-019-0429-1

pISSN: 0256-1115
eISSN: 1975-7220

Gas hydrate formation by allyl alcohol and CH_4: Spectroscopic and thermodynamic analysis

Ki Hun Park and Minjun Cha†

Department of Energy and Resources Engineering, Kangwon National University,
1 Kangwondaehak-gil, Chuncheon-si, Gangwon-do 24341, Korea
(*Received 25 July 2019 • accepted 12 November 2019*)

Abstract−We discovered a new structure II (sII) hydrate forming agent, allyl alcohol (AA), in the presence of methane (CH_4) for the first time, and characterized the crystal structure, guest distribution, and phase equilibria of the (AA+CH_4) hydrate. Using solid-state ^{13}C NMR and Raman spectroscopy, the crystal structure of the (AA+CH_4) hydrate was confirmed to be a sII hydrate, and the CH_4 molecule was found to be encapsulated in both the large and small cages of the sII hydrate. In addition, AA was found to be included in the large cages of the sII hydrate in the *Gauche-Gauche* form based on the measured- and calculated-NMR spectra. Notably, we investigated the free OH signal of AA in the Raman spectra to determine whether hydrogen bonding occurred between host and guest molecules; however, we could not determine whether the existence of the free OH signal was consistent with this host-guest interaction. To clearly identify the crystal structure and possible host-guest interactions, a high-resolution powder X-ray diffraction (HRPD) pattern of our (AA+CH_4) hydrate sample was analyzed using Rietveld analysis with the direct space method. The crystal structure of the (AA+CH_4) hydrate was assigned as the cubic *Fd3m* structure with a lattice constant of 17.1455 Å. In particular, the shortest distance between the AA molecule in the hydrate cages and an oxygen atom in the host water was estimated to be 2.55 Å; thus, we concluded that the hydroxyl group of the AA molecule was hydrogen-bonded to the host water framework. Finally, we measured the phase equilibrium conditions of the binary (AA+CH_4) hydrate and found that the equilibrium pressure conditions of the binary (AA+CH_4) hydrate were slightly higher than those of the pure CH_4 hydrate.

Keywords: Gas Hydrate, Phase Equilibria, Structure Identification, Allyl Alcohol, Hydrogen Bonding

INTRODUCTION

Clathrate hydrates, also known as gas hydrates, are ice-like compounds composed of hydrogen-bonded water molecules forming 'host' cages that encapsulate 'guest' molecules [1,2]. In general, there are three well-known hydrate structures: cubic structure I, cubic structure II, and hexagonal structure H [1,2]. All three have the same small (5^{12}) cages but different large cages in their structures. The relative size of the hydrate cage and the guest molecule are the key factors that determine the hydrate structure and hydrate cage occupancy; thus, small gaseous guest molecules (e.g., methane, ethane, nitrogen, oxygen, and hydrogen) as well as large organic guest molecules (e.g., cyclopentane, tetrahydrofuran, and 2,2-dimethyl butane) can be selectively captured in hydrate cages [1-13]. Clathrate hydrates can be applied in various fields, including gas storage and transportation [13-18], greenhouse gas control [19-23], carbon capture and sequestration [24-27], and desalination [18,28-33]. Thus, clathrate hydrates are an option for future sustainable development.

Clathrate hydrates can be formed under low-temperature and high-pressure conditions, and thus, clathrate hydrate formation is a serious issue during the oil and gas production process [1,2]. Simple alcohols, mainly methanol, are often used as thermodynamic hydrate inhibitors as these alcohols form strong hydrogen bonds with water [3,34-39]. However, some monohydroxy alcohols, such as propanols, butanols, and pentanols, can play multiple distinct roles in the formation of clathrate hydrates, as the hydrophobic-hydrophilic balance shifts as the size of the alkyl group increases [40-49]. Therefore, several large monohydroxy alcohol molecules, such as 1-propanol [44,45,50], 2-propanol [44,51-53], 1-butanol [48], *iso*-butanol [48], *tert*-butanol [48], 3-methyl-1-butanol [40], 2,2-dimethyl-1-propanol [40], 3-methyl-2-butanol [40], and 2-methyl-2-butanol [40] have been identified as cubic structure type II (sII) or hexagonal structure (sH) hydrate-forming agents in the presence of a helping gas. Although these large alcohol molecules can be regarded as hydrate formers, they still contain a monohydroxy group in their structures. Therefore, possible hydrogen bonding interactions between the guest and host molecules have been examined by several researchers. Cha et al. [40] reported that possible guest-host hydrogen bonding interactions can be investigated through the observation of free OH signals in Raman spectroscopy. Molecular dynamics simulations have also been used to demonstrate possible guest-host hydrogen bonding interactions and have indicated that long-lived hydrogen bonding can occur in hydrate cages [44]. More recently, Takeya et al. [54] attempted the *ab initio* crystal structural determination of gas hydrate structures using Rietveld analysis with the direct-space method from the powder X-ray diffraction pattern; their results provided useful insights into understanding the complex nature of host-guest chemistry.

†To whom correspondence should be addressed.
E-mail: minjun.cha@kangwon.ac.kr

The aim of the present study was to discover a new structure II hydrate-forming agent and to identify any guest-host interactions occurring in the resulting clathrate hydrate system. We investigated the crystal structure, guest distribution, and possible guest-host interactions in the (allyl alcohol+methane) hydrate for the first time using spectroscopic techniques. ^{13}C solid-state NMR and Raman spectroscopy were used to identify the crystal structure of the hydrate, and the high-resolution powder X-ray diffraction pattern of the (AA+CH_4) hydrate was refined using Rietveld analysis with the direct space method to search for possible guest-host interactions in the hydrate cages. Finally, the thermodynamic conditions of the (AA+CH_4) hydrate were examined using the conventional isochoric method.

EXPERIMENTAL DETAILS

Allyl alcohol (AA, CH_2CHCH_2OH) with a minimum purity of 99.0 mol% was purchased from Sigma-Aldrich. Methane (CH_4) gas with a minimum purity of 99.95 mol% was supplied by Deokyang Corporation. Distilled water was used to prepare the AA solution (5.6 mol%).

The allyl alcohol (AA) solution (5.56 mol%) was stored in a freezer at approximately 203 K and atmospheric pressure. The frozen solution was crushed with a 100-μm sieve under liquid nitrogen conditions. The powdered sample was placed into a high-pressure reactor, which was then pressurized to 10 MPa with CH_4 and maintained at 263 K for a week in a bath circulator. After the hydrate was formed, the reactor was soaked in liquid nitrogen and loaded CH_4 gas was released carefully to prevent hydrate dissociation. The formed hydrate was crushed again using the 100 μm sieve. The resulting powdered hydrate sample was used for solid-state NMR, Raman spectroscopy, and high-resolution powder X-ray diffraction.

The ^{13}C solid-state high-power proton-decoupled (HPDEC) magic angle spinning (MAS) NMR spectrum was obtained to identify the hydrate structure and the guest distribution of binary (allyl alcohol+CH_4) hydrate using a Bruker AVANCE II+ 400 MHz NMR instrument at the KBSI Seoul Western Center. The hydrate powder was loaded into a zirconia rotor with an outer diameter of 4 mm, which was then placed into the NMR instrument, which was cooled to 200 K. The ^{13}C frequency of the spectrometer was 100.4 MHz. All measurements were performed at a MAS speed of 3 kHz, using a pulse length of 1.5 μs and a delay time of 10 s. As the chemical shift reference, the TMS signal was calibrated to a chemical shift of 0 ppm.

A dispersive Raman spectrometer (ARAMIS, Horiba Jobin Yvon Inc., France) was used to examine the crystal structure, guest distribution, and possible host-guest interactions of the binary (allyl alcohol+CH_4) hydrate. All measurements were collected at the Central Laboratory of Kangwon National University (Chuncheon-si). An Ar-ion laser source with a wavelength of 514.53 nm was used; the laser intensity was approximately 30 mW. A temperature-controlled stage (THMS600G, LINKAM) was used to control the temperature.

High resolution powder diffraction (HRPD) at beamline 9B at the Pohang Accelerator Laboratory (PAL, Republic of Korea) was used to investigate the crystal structure of the binary (allyl alcohol+CH_4) hydrate. The wavelength of the beam was 1.5173 Å, and the HRPD pattern of the binary (allyl alcohol+CH_4) hydrate was acquired at 80 K with a fixed time of 2 s and a step size of 0.01° for 2θ=0-120°. We refined the obtained pattern using the program FULLPROF for the Rietveld analysis [55]. The initial position of AA molecule in the large cages of sII hydrate was checked using FOX program with the direct space method [56]. Atomic scattering factors were added to demonstrate the virtual species for H_2O, CH_4, -CH_2-, -CH-, and -OH groups [54,57].

The conventional isochoric method to trace the pressure and temperature data was used to measure the phase equilibrium conditions of the binary (allyl alcohol+CH_4) hydrate [38,58]. The AA solution (5.6 mol%) was loaded into a pressure reactor (316 stainless steel) with a magnetically coupled stirrer. The pressure reactor was sealed and placed in a bath circulator. After flushing with CH_4 gas, the reactor was pressurized to sufficient pressure (12.0 MPa) using CH_4 gas at room temperature. The temperature of the bath circulator was set to 285.15 K. The detailed experimental procedure for measuring the phase equilibria of the hydrate system was as follows: (1) fast cooling (2 K/h in a step-wise manner), (2) hydrate formation via a sudden pressure drop, (3) fast heating (0.5 K/h in a step-wise manner), and (4) slow heating (0.1 K/h in a stepwise manner).

RESULTS AND DISCUSSION

The shape of the large guest molecules and the relative size of

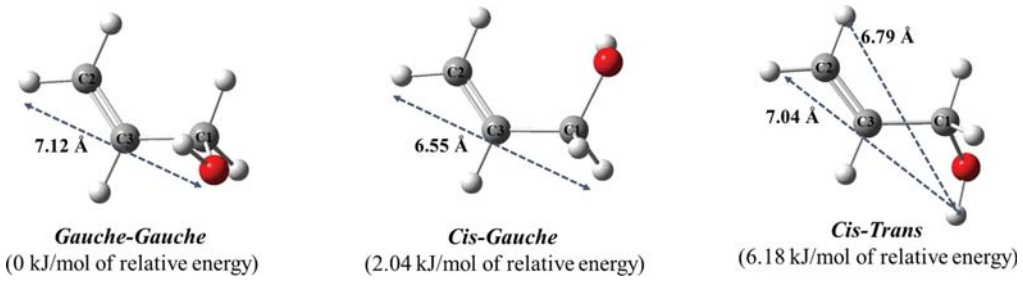

Fig. 1. Conformation of allyl alcohol and their molecular sizes (Grey, carbon; white, hydrogen; red, oxygen). In addition, the end-to-end distances of allyl alcohol are also calculated by adding the van der Waals radius of the H (1.20 Å) or O atom (1.52 Å) at each end [1,2]. First letter (*Gauche* or *Cis*) indicates the relative position of the hydroxyl group to the C=C bond (C-C-C-O angle), and second letter (*Gauche* or *Trans*) represents the relative position of the hydroxyl group (C-C-O-H angle).

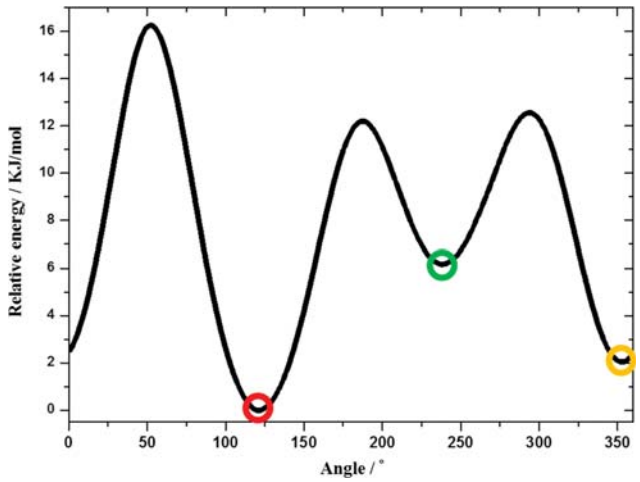

Fig. 2. Scan of total energy of allyl alcohol molecule depending on the angle between the atoms (red circle, the lowest energy, *Gauche-Gauche* form; orange circle, the second lowest energy, C*is-Gauche* form; green circle, the third lowest energy, *Cis-Trans* form).

the hydrate cage to the guest molecule are considered to be the key parameters for estimating the hydrate structure in the presence of large guest molecules and help guests [1,2,59]. To examine the shape and size of the allyl alcohol molecules, three possible conformations of allyl alcohol were optimized in the program Gaussian 03 [60] using the B3LYP model and the 6-311++ G (d, p) basis set (Fig. 1). In addition, the potential energy surface (PES) of allyl alcohol was also calculated using Gaussian 03 (Fig. 2). Fig. 1 shows the three possible conformations of the allyl alcohol (*Gauche-Gauche* form, *Cis-Gauche* form, and *Cis-Trans* form). The end-to-end lengths of allyl alcohol were also calculated by adding the van der Waals radius of the H (1.20 Å) or O atom (1.52 Å) at each end [1,2].

The molecular size of allyl alcohol in the *Gauche-Gauche* form (7.12 Å) was larger than in the *Cis-Gauche* form (6.55 Å) or the *Cis-Trans* form (7.04 Å). As the size of allyl alcohol ranged from 6.55 to 7.12 Å (Fig. 1), we expected that a structure II (sII) or structure H (sH) hydrate could be formed in the presence of a help guest [1,2]. The relative energies (i.e., the calculated difference in the potential energy between a given conformer and the conformer having the lowest potential energy) of the three allyl alcohol conformations are also shown in Fig. 1. The *Gauche-Gauche* form (relative energy: 0 kJ/mol) of allyl alcohol was the most stable conformation. The C*is-Gauche* form (relative energy: 2.04 kJ/mol) and the *Cis-Trans* form (relative energy: 6.18 kJ/mol) were less stable; thus, the *Gauche-Gauche* form was expected to be the preferred conformation of allyl alcohol in the hydrate cages based on its low potential energy. However, the relative energy differences among the three conformations were small (Fig. 1 and 2), and all three conforma-

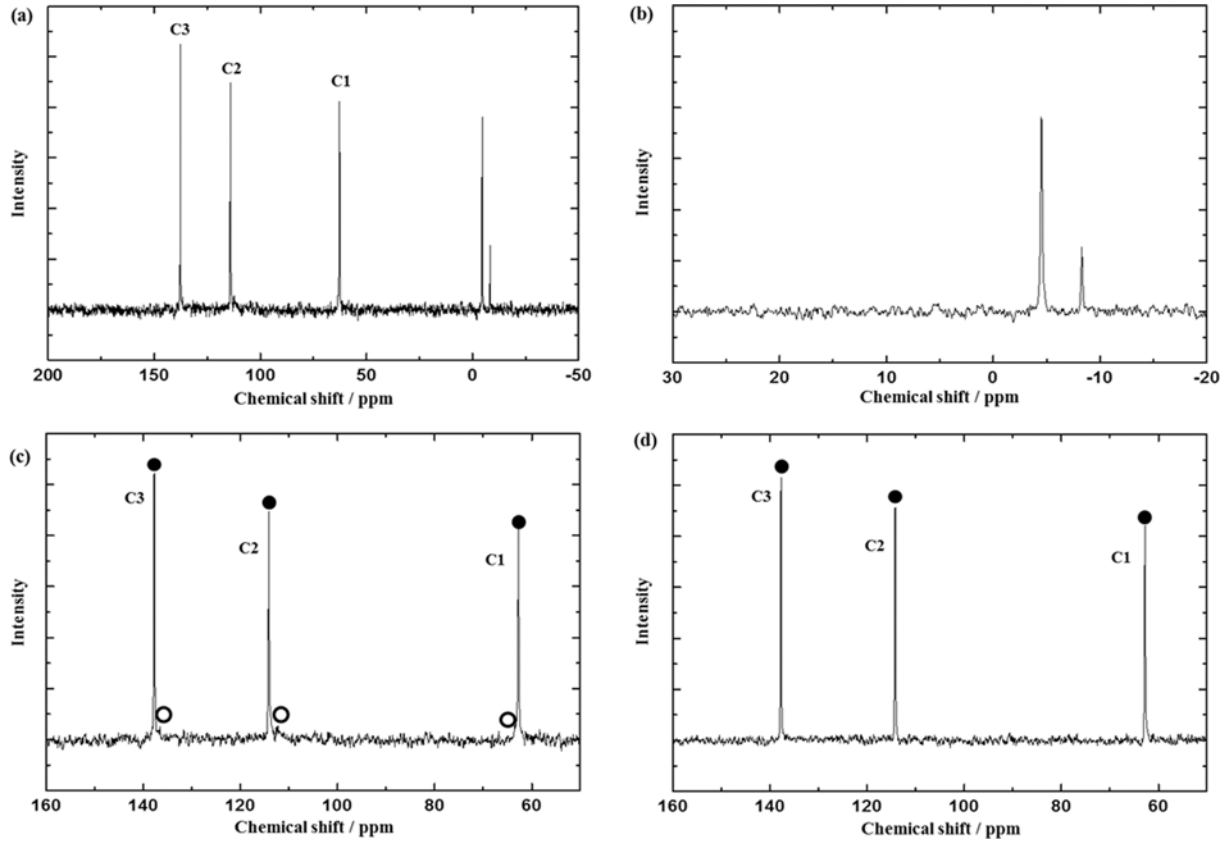

Fig. 3. ^{13}C NMR spectra of (a) allyl alcohol+CH_4 hydrate for full range, (b) allyl alcohol+CH_4 hydrate for CH_4 regions, (c) allyl alcohol+CH_4 hydrate for allyl alcohol regions, and (d) allyl alcohol+H_2O system for allyl alcohol regions. Filled circles indicate chemical shifts of allyl alcohol for allyl alcohol+H_2O system, while white circles represent chemical shifts of allyl alcohol in hydrate phase.

Table 1. Measured and calculated chemical shifts (ppm) of conformers of allyl alcohol

Carbon label	AA+H_2O	AA+CH_4 hydrate	*Gauche-Gauche*	*Cis-Gauche*	*Cis-Trans*
C1	62.7	~63.4	70.14	67.41	69.64
C2	114.1	~113.5	120.62	114.17	120.57
C3	137.7	~136.6	147.96	147.98	146.88

tions could possibly be enclathrated into the large cages of a sII or sH hydrate. At this stage, we could not predict whether the *Gauche-Gauche* form of allyl alcohol was most likely to be present in the large cages of the hydrate structure.

We analyzed the ^{13}C solid-state HPDEC MAS NMR spectrum of the binary (allyl alcohol+CH_4) hydrate at 200 K to confirm the crystal structure and guest behavior of our hydrate system. Additionally, the geometric conformation of allyl alcohol in the large cages of the hydrate structure was also investigated by comparing the measured and calculated NMR spectra. Fig. 3 shows the NMR spectra of the binary (allyl alcohol+CH_4) hydrate (Fig. 3(a)-3(c)) and that of the frozen allyl alcohol solution for comparison (Fig. 3(d)). In Fig. 3(b), two striking peaks that were representative of entrapped CH_4 molecules in the 5^{12} small cage (sII-S, δ=−4.5 ppm) and the $5^{12}6^4$ large cage (sII-L, δ=−8.3 ppm) of structure II (sII) are observed. The peak area ratio of the entrapped CH_4 molecules ($A_{sII\text{-}S}/A_{sII\text{-}L}$) is 3.7, as shown in Fig. 3(b). This ratio allows us to confirm the presence of allyl alcohol in the large cages of the sII hydrate [1,2].

Although a 5.6 mol% allyl alcohol solution, which represented a 1 : 1 stoichiometry with the large cages of the sII hydrate, was used to synthesize the binary (allyl alcohol+CH_4) hydrate (sII hydrate) in this study, the large cages of the sII hydrate were not fully occupied by allyl alcohol, implying that some of the $5^{12}6^4$ large cages were occupied by CH_4 (as demonstrated by the sII-L peak at δ= −8.3 ppm) due to the inhomogeneity of the allyl alcohol solution during hydrate formation (Fig. 3(a) and 3(b)). Therefore, some unreacted allyl alcohol remained, as shown in Fig. 3(c) (filled circles). In Fig. 3(d), the NMR spectrum of the frozen allyl alcohol solution is shown for comparison. Three representative peaks were observed at approximately δ=62.7, 114.1, and 137.7 ppm (filled circles). After hydrate formation, the allyl alcohol captured in the large cages of sII hydrate gave rise to peaks at approximately δ=63.4, 113.5, and 136.6 ppm (white circles); the chemical shifts of these peaks were similar, although slightly different, to those of the frozen allyl alcohol solution sample. The intensities of the captured allyl alcohol in the large cages of the sII hydrate were much lower than those of the unreacted allyl alcohol; thus, our synthesized hydrate sample included a large fraction of frozen allyl alcohol solution as an impurity. To clearly demonstrate the captured allyl alcohol in the large cages of sII hydrate, expansions of the NMR peaks are shown in the Fig. S1 and S2. However, the peak intensity of captured-allyl alcohol (white circle in Fig. 3) appears to be similar intensity as the noise, so we cannot rule out the possibility of overlapped-peak in frozen allyl alcohol and captured allyl alcohol.

To clarify the conformation of the allyl alcohol molecule in the large cages of the sII hydrate, the chemical shifts of the allyl alcohol molecules were calculated for each allyl alcohol conformer using density functional theory with the B3LYP model and the 6-311++G (d,p) basis set in Gaussian 03 [60]. The observed chemical shifts (from Fig. 3) and calculated chemical shifts were tabulated. As shown in Fig. 3(d) and Table 1, three peaks were observed in the ^{13}C spectrum of frozen allyl alcohol at approximately δ= 62.7, 114.1, and 137.7 ppm (Fig. 3(d)); these values were most similar to the calculated chemical shifts (the chemical shift difference between C1 and C2 or C2 and C3) of the *Gauche-Gauche* and *Cis-Trans* conformations of allyl alcohol (Table 1). After hydrate formation, the chemical shifts of the allyl alcohol captured in the hydrate cages were observed at δ=63.4, 113.5, and 136.6 ppm (Fig. 3(c)), and were also similar to the chemical shifts calculated for the *Gauche-Gauche* and *Cis-Trans* form of allyl alcohol. Thus, we concluded that the allyl alcohol did not undergo conformational change during hydrate formation. Notably, the relative potential energy difference between the *Gauche-Gauche* and the *Cis-Trans* form of allyl alcohol was 6.18 kJ/mol (Fig. 1), and the energy barrier between the *Gauche-Gauche* and *Cis-Trans* conformations was calculated to be large (Fig. 2). Therefore, it is reasonable to assume that the allyl alcohol molecules in the large cages of the sII hydrate were in the *Gauche-Gauche* conformation.

The Raman spectrum of the binary (allyl alcohol+CH_4) hydrate was also acquired to investigate the behavior of the guests in the hydrate cages. Similar to in the ^{13}C HPDEC NMR spectra, we observed two prominent Raman peaks at 2,902 cm^{-1} and 2,913 cm^{-1}, which corresponded to CH_4 molecules captured in the small 5^{12} and large $5^{12}6^4$ large cages of an sII hydrate structure [1,2]. Further-

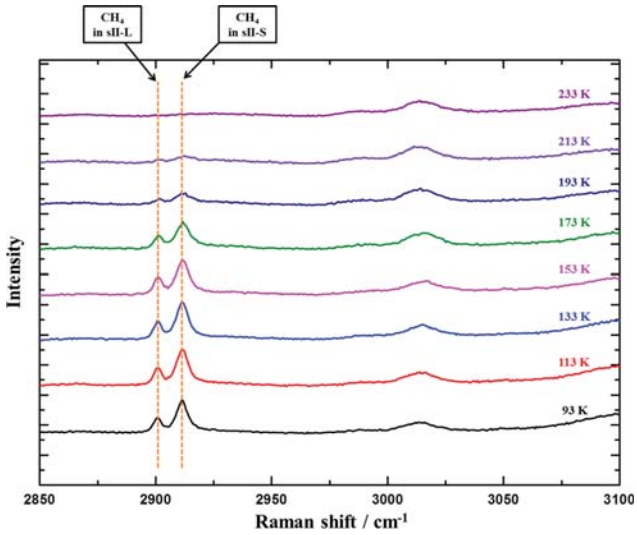

Fig. 4. Raman spectra of allyl alcohol+CH_4 hydrate measured at various temperatures.

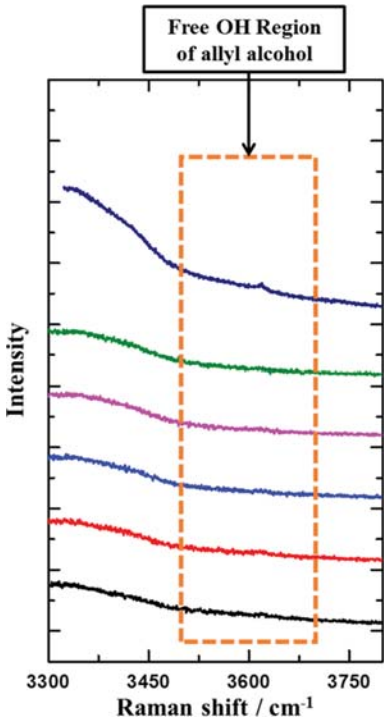

Fig. 5. Raman spectra of allyl alcohol+CH_4 hydrate measured at various spots (93 K).

more, the dissociation behavior of the binary (allyl alcohol+CH_4) hydrate was also studied at temperatures from 93 K to 233 K under atmospheric pressure. From 93 to 173 K, no significant changes in the Raman signals of the captured CH_4 molecules in the 5^{12} and $5^{12}6^4$ cages were observed (Fig. 4). At atmospheric pressure, the dissociation of the binary (allyl alcohol+CH_4) hydrate began at 193 K and was complete at 233 K.

Fig. 5 shows Raman spectra of the binary (allyl alcohol+CH_4) hydrate measured at various spots (93 K) to investigate possible guest-host interactions via hydrogen bonding. In previous studies, the absence of the 'free OH' signal in the Raman spectrum at around 3,600 cm^{-1} was associated with long-lived hydrogen bonding interactions between the guest and host molecules [40,48]. As shown in Fig. 5, six measurements were performed to check for the existence of 'free OH' signals at various spots, and a small signal was observed at around 3,619 cm^{-1}. Although we identified a small 'free OH' signal in our Raman spectra, it was difficult to conclude whether the allyl alcohol captured in the large cages of sII hydrate participated in guest-host hydrogen bonding, because a large portion of unreacted allyl alcohol was still present. The average size of the large cages in an sII hydrate is estimated to be 6.66 Å; the *Gauche-Gauche* form of the allyl alcohol molecule was slightly larger (7.12 Å) than the average size of the large cages. Thus, structural analysis of our hydrate sample was required to investigate the possible guest-host hydrogen bonding interaction [54,57,61].

To confirm the guest behavior of the binary (allyl alcohol+CH_4) hydrate and to understand the possible guest-host interactions in the large cages of the sII hydrate, a high-resolution synchrotron X-ray diffraction (HRPD) pattern of the hydrate sample was acquired from beamline 9B at the Pohang Accelerator Laboratory (PAL) and refined using Rietveld analysis with the direct space method. The position of the allyl alcohol molecule in the large cages of the sII hydrate was analyzed using the direct space method, and atomic scattering factors were added to demonstrate the virtual species for H_2O and the CH_4, -CH_2-, -CH-, and -OH groups [54,57,61]. Table 2 summarizes the atomic coordinates, site occupancies, and isotropic thermal factors obtained using Rietveld analysis. During structure refinement, the site occupancy ratio for the captured CH_4 molecules in the small and large cages of the sII hydrates ($A_{sII\text{-}S}$/$A_{sII\text{-}L}$) was set as 3.7 (Fig. 3(b)).

Fig. 6(a) shows the synchrotron HRPD pattern of the binary (allyl alcohol+CH_4) hydrate measured at 80 K and the Rietveld refinement results (background corrected R_{wp}=19.4% and χ^2=5.25). The tick marks in Fig. 6(a) indicate the Bragg positions of the sII hydrate (top, blue) and hexagonal ice (bottom, red). The lower blue line shown in Fig. 6(a) represents the difference between the measured (red points in Fig. 6(a)) and refined (black line in Fig. 6(a)) HRPD pattern. The three notable peaks between 22 and 26° (red tick marks) corresponded to hexagonal ice. The relative intensities of these ice peaks were much stronger than those of the hydrate peaks; thus, we concluded that our synthesized hydrate sample included a large fraction of frozen allyl alcohol solution as an impurity. The weight fractions of the sII hydrate and hexagonal ice phases were calculated to be 45.75 (0.46) and 54.25 (0.43), respectively. The refined HRPD patterns indicated the formation of a cubic

Table 2. Atomic coordinates and isotropic temperature factors for allyl alcohol+CH_4 hydrate

Atom	x	y	z	B (Å^2)	Site occupancy
Wa1 (H_2O)	0.1250	0.1250	0.1250	5.1968	8.0000
Wa2 (H_2O)	0.2176	0.2176	0.2176	4.7721	32.0000
Wa3 (H_2O)	0.1822	0.1822	0.3709	5.8208	96.0000
Ms (CH4 in 5^{12} cage)	0.9982	0.7505	0.7097	4.4394	14.9439
Ml (CH4 in $5^{12}6^4$ cage)	0.3750	0.3750	0.3750	22.3004	4.5749
LG1 (CH_2 in AA)	0.3897	0.4469	0.4314	8.51	3.9300
LG2 (CH in AA)	0.3566	0.3767	0.4303	8.51	3.9300
LG3 (CH_2 in AA)	0.3470	0.3280	0.3582	8.51	3.9300
LG4 (OH in AA)	0.3843	0.2537	0.3650	8.51	3.9300

[a]The position of methane in the sII-L was confined to the center of cage during the refinement

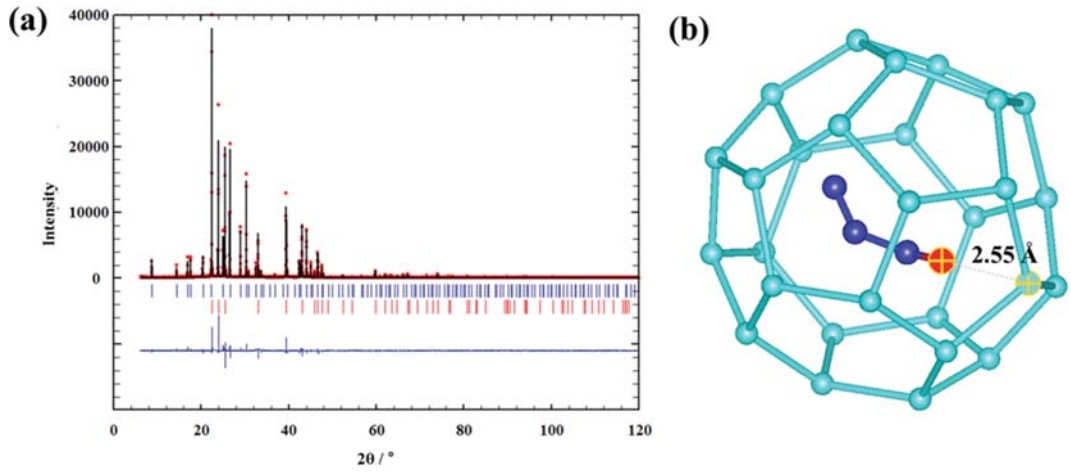

Fig. 6. (a) Synchrotron HRPD pattern of allyl alcohol+CH_4 hydrate measured at 80 K and the Rietveld refinement results (background corrected R_{wp}=19.4% and χ^2=5.25). Tick marks indicate the Bragg position for sII hydrate (top) and the hexagonal ice (bottom). (b) The allyl alcohol in the $5^{12}6^4$ cage of sII hydrate (carbon in hydrocarbon group of allyl alcohol molecule, blue; oxygen in hydroxyl group of allyl alcohol molecule, red; oxygen in water host molecule, light-blue).

Fd3m structure with a lattice constant of 17.14565(16) Å. In Fig. 6(b), the shortest distance between a 'host' water and 'guest' allyl alcohol molecule was determined to be 2.55 Å (Fig. 6(b)), and this host - guest distance is in the range of O-O distances consistent with hydrogen bonding; thus, we tentatively concluded that long-lived guest-host hydrogen bonding interactions existed [54,57,61].

Table 3. Equilibrium temperature and pressure conditions of allyl alcohol+CH_4 hydrate

Allyl alcohol (5.6 mol%)+CH_4 hydrate	
Temperature (K)	Pressure (MPa)
271.85	2.21
278.74	4.84
281.15	6.52
282.16	7.45
284.35	9.74
285.54	11.25

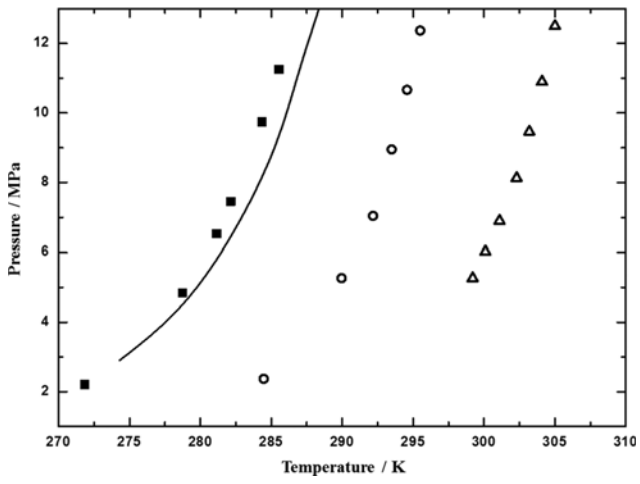

Fig. 7. Phase equilibrium curve of allyl alcohol (5.6 mol%)+CH_4 (■), pure CH_4 (black line) [1,2], THF (5 mol%)+CH_4 (△) [7], methacrolein (5.56 mol%)+CH_4 (○) hydrates[62].

Finally, we also measured the phase equilibrium conditions of the binary (allyl alcohol+CH_4) hydrate in the temperature range 270.0-285.5 K and the pressure range 2.0-11.5 MPa; the equilibrium pressure conditions are listed in Table 3 and presented in Fig. 7. The equilibrium temperatures of the binary (allyl alcohol+CH_4) hydrate were slightly lower than those of the pure CH_4 hydrate for a given pressure condition [1]. In addition, the thermodynamic conditions of the binary (allyl alcohol+CH_4) hydrate were also more unstable than those of binary (tetrahydrofuran+CH_4) and (methacrolein+CH_4) hydrates [7,62].

CONCLUSIONS

The crystal structure, guest distribution, and phase equilibria of the binary (allyl alcohol+CH_4) hydrate were investigated for the first time. NMR spectra confirmed the formation of a structure II hydrate in the presence of allyl alcohol and CH_4. In addition, the CH_4 molecule was found to be encapsulated in both the large and small cages of the sII hydrate, and the AA in the large cages of the sII hydrate was concluded to be in the *Gauche-Gauche* form. Raman spectra of the (allyl alcohol+CH_4) hydrate also supported the formation of the structure II hydrate. To identify possible host-guest interactions, a high-resolution powder X-ray diffraction (HRPD) pattern of our (allyl alcohol+CH_4) hydrate sample was analyzed using Rietveld analysis with the direct space method. The structure refinement confirmed that the AA molecule was located in the large cages of the structure II hydrate, and the shortest distance between the AA molecule in the hydrate cages and an oxygen atom of the host water molecules was found to be 2.55 Å, indicating a possible host-guest interaction. Finally, we also measured the phase equilibrium conditions of the binary (allyl alcohol+CH_4) hydrate, and found that the equilibrium pressure conditions of the binary (allyl alcohol+CH_4) hydrate were slightly higher than those of the pure CH_4 hydrate.

ACKNOWLEDGEMENT

This study was supported by the National Research Foundation of Korea (NRF) grants (NRF-2017R1C1B5017036 and NRF-2019R1F1A1058167) funded by the Korea government (MSIT; Ministry of Science and ICT). NMR experiments are acquired at Bruker AVANCE II+ 400 MHz NMR system in KBSI Seoul Western Center. High resolution powder diffraction (HRPD) patterns are collected from the beamline (9B) at Pohang Accelerator Laboratory.

SUPPORTING INFORMATION

Additional information as noted in the text. This information is available via the Internet at http://www.springer.com/chemistry/journal/11814.

REFERENCES

1. E. D. Sloan and C. A. Koh, *Clathrate Hydrates of Natural Gases*, 3rd Ed. CRC Press Boca Raton (2008).
2. E. D. Sloan, *Nature*, **426**, 353 (2003).
3. M. Cha, K. Shin, J. Kim, D. Chang, Y. Seo, H. Lee and S. P. Kang, *Chem. Eng. Sci.*, **99**, 184 (2013).
4. H. Mimachi, S. Takeya, A. Yoneyama, K. Hyodo, T. Takeda, Y. Gotoh and T. Murayama, *Chem. Eng. Sci.*, **118**, 208 (2014).
5. H. P. Veluswamy, A. Kumar, Y. Seo, J. D. Lee and P. Linga, *Appl. Energy*, **216**, 262 (2018).
6. Z. M. Aman, E. P. Brown, E. D. Sloan, A. K. Sum and C. A. Koh, *Phys. Chem. Chem. Phys.*, **13**(44), 19796 (2011).
7. Y.-T. Seo, S.-P. Kang and H. Lee, *Fluid Phase Equilib.*, **189**, 99 (2001).
8. Y. Seo, S. P. Kang, J. Lee, J. Seol and H. Lee, *J. Chem. Eng. Data*, **56**(5), 2316 (2011).
9. Y. Jin, M. Kida and J. Nagao, *J. Phys. Chem. C*, **119**(17), 9069 (2015).
10. S. Muromachi, T. Nakajima, R. Ohmura and Y. H. Mori, *Fluid Phase Equilib.*, **305**(2), 145 (2011).
11. K. Shin, M. Cha, W. Lee, H. Kim, Y. Jung, J. Dho, J. Kim and H. Lee, *J. Am. Chem. Soc.*, **133**(50), 20399 (2011).
12. L. J. Florusse, C. J. Peters, J. Schoonman, K. C. Hester, C. A. Koh, S. F. Dec, K. N. Marsh and E. D. Sloan, *Science*, **306**(5695), 469 (2004).
13. K. A. Lokshin, Y. S. Zhao, D. W. He, W. Mao, H. K. Mao, R. J. Hemley, M. V. Lobanov and M. Greenblatt, *Abstr. Pap. Am. Chem. S*, **229**, U589 (2005).
14. W. X. Wang, C. L. Bray, D. J. Adams and A. I. Cooper, *J. Am. Chem. Soc.*, **130**(35), 11608 (2008).
15. T. Daitoku and Y. Utaka, *Appl. Energy*, **87**(8), 2682 (2010).
16 N. J. Kim, J. H. Lee, Y. S. Cho and W. Chun, *Energy*, **35**(6), 2717 (2010).
17. B. S. Kiran, K. Sowjanya, P. S. R. Prasad and J. H. Yoon, *Oil Gas Sci. Technol.*, **74**, 12 (2019).
18. Z. R. Chong, T. B. He, P. Babu, J. N. Zheng and P. Linga, *Desalination*, **463**, 69 (2019).
19. S. J. Obrey, R. P. Currier, F. F. Jebrail, L. A. Le, R. J. Martinez, M. A. Sedillo, D. L. Yang, S. Tam, G. Deppe, A. Lee and D. F. Spencer, *Abstr. Pap. Am. Chem. S*, **231**, INOR237 (2006).
20. J. Park, Y. T. Seo, J. W. Lee and H. Lee, *Catal. Today*, **115**(1-4), 279 (2006).
21. Y. Park, D. Y. Kim, J. W. Lee, D. G. Huh, K. P. Park, J. Lee and H. Lee, *Proc. Natl. Acad. Sci. USA*, **103**(34), 12690 (2006).
22. H. J. Lee, J. D. Lee and Y. D. Kim, *Kor. J. Mater. Res.*, **18**(12), 650 (2008).
23. Y. J. Yang, D. Shin, S. Choi, Y. Woo, J. W. Lee, D. Kim, H. Y. Shin, M. Cha and J. H. Yoon, *Environ. Sci. Technol.*, **51**(6), 3550 (2017).
24. D. Y. Koh, H. Kang, D. O. Kim, J. Park, M. Cha and H. Lee, *Chemsuschem.*, **5**(8), 1443 (2012).
25. K. Shin, Y. Park, M. J. Cha, K. P. Park, D. G. Huh, J. Lee, S. J. Kim and H. Lee, *Energy Fuel*, **22**(5), 3160 (2008).
26. A. Farhadi and V. Mohebbi, *Int. J. Hydrogen Energy*, **42**(31), 19967 (2017).
27. Y. Youn, M. J. Cha, M. Kwon, J. Park, Y. Seo and H. Lee, *Korean J. Chem. Eng.*, **33**(5), 1712 (2016).
28. S. D. Seo, S. Y. Hong, A. K. Sum, K. H. Lee, J. D. Lee and B. R. Lee, *Chem. Eng. J.*, **370**, 980 (2019).
29. W. Choi, Y. Lee, J. Mok, S. Lee, J. D. Lee and Y. Seo, *Chem. Eng. J.*, **358**, 598 (2019).
30. H. Lee, H. Ryu, J. H. Lim, J. O. Kim, J. D. Lee and S. Kim, *Desalin Water Treat.*, **57**(19), 9009 (2016).
31. K. C. Kang, P. Linga, K. N. Park, S. J. Choi and J. D. Lee, *Desalination*, **353**, 84 (2014).
32. J. H. Cha and Y. Seol, *Acs Sustain. Chem. Eng.*, **1**(10), 1218 (2013).
33. K. N. Park, S. Y. Hong, J. W. Lee, K. C. Kang, Y. C. Lee, M. G. Ha and J. D. Lee, *Desalination*, **274**(1-3), 91 (2011).
34. M. Cha, K. Shin, Y. Seo, J. Y. Shin and S. P. Kang, *J. Phys. Chem. A*, **117**(51), 13988 (2013).
35. M. J. Cha, S. Baek, H. Lee and J. W. Lee, *Rsc Adv.*, **4**(50), 26176 (2014).
36. M. J. Cha, S. Baek, J. Morris and J. W. Lee, *Chem-Asian J.*, **9**(1), 261 (2014).
37. M. J. Cha, A. Couzis and J. W. Lee, *Langmuir*, **29**(19), 5793 (2013).
38. M. J. Cha, Y. Hu and A. K. Sum, *Fluid Phase Equilib.*, **413**, 2 (2016).
39. M. J. Cha, H. Lee and J. W. Lee, *J. Phys. Chem. C*, **117**(45), 23515 (2013).
40. M. Cha, K. Shin and H. Lee, *J. Phys. Chem. B*, **113**(31), 10562 (2009).
41. S. Alavi, K. Shin and J. A. Ripmeester, *J. Chem. Eng. Data*, **60**(2), 389 (2015).
42. K. Shin, K. A. Udachin, I. L. Moudrakovski, D. M. Leek, S. Alavi, C. I. Ratcliffe and J. A. Ripmeester, *Proc. Natl. Acad. Sci. USA*, **110**(21), 8437 (2013).
43. J. W. Lee and S. P. Kang, *J. Phys. Chem. B*, **116**(1), 332 (2012).
44. S. Alavi, S. Takeya, R. Ohmura, T. K. Woo and J. A. Ripmeester, *J. Chem. Phys.*, **133**(7), 074505 (2010).
45. M. Cha, K. Shin and H. Lee, *Korean J. Chem. Eng.*, **34**(9), 2514 (2017).
46. R. Ohmura, S. Takeya, T. Uchida, I. Y. Ikeda, T. Ebinuma and H. Narita, *Fluid Phase Equilib.*, **221**(1-2), 151 (2004).
47. S. Sinehbaghizadeh, J. Javanmardi and A. H. Mohammadi, *J. Chem. Thermodyn.*, **125**, 64 (2018).
48. Y. Youn, M. Cha and H. Lee, *Chemphyschem.*, **16**(13), 2876 (2015).

49. F. V. Zhurko, A. Y. Manakov and V. I. Kosyakov, *Chem. Eng. Sci.*, **65**(2), 900 (2010).
50. K. Udachin, S. Alavi and J. A. Ripmeester, *J. Chem. Phys.*, **134**(12), 054702 (2011).
51. M. Imai, Y. Oto, S. Nitta, S. Takeya and R. Ohmura, *J. Chem. Thermodyn.*, **47**, 17 (2012).
52. S. Imai, K. Miyake, R. Ohmura and Y. H. Mori, *J. Chem. Eng. Data*, **52**(3), 1056 (2007).
53. R. Ohmura, S. Takeya, T. Uchida and T. Ebinuma, *Ind. Eng. Chem. Res.*, **43**(16), 4964 (2004).
54. S. Takeya, K. A. Udachin, I. L. Moudrakovski, R. Susilo and J. A. Ripmeester, *J. Am. Chem. Soc.*, **132**(2), 524 (2010).
55. J. Rodríguez-Carvajal, *Phys. B: Condens. Matter*, **192**, 55 (1993).
56. V. Favre-Nicolin and R. Černý, *J. Appl. Crystallogr.*, **35**, 734 (2002).
57. Y. H. Ahn, B. Lee and K. Shin, *Crystals*, **8**(8), 328 (2018).
58. K. H. Park, D. Jeong, J. H. Yoon and M. Cha, *Fluid Phase Equilib.*, **493**, 43 (2019).
59. K. Shin, Y. Park, J. H. Hong and H. Lee, *Korean J. Chem. Eng.*, **24**(5), 843 (2007).
60. M. J. Frisch, G. W. Trucks, H. B. Schlegel, G. E. Scuseria, M. A. Robb, J. R. Cheeseman, J. A. Montgomery, Jr., T. Vreven, K. N. Kudin, J. C. Burant, J. M. Millam, S. S. Iyengar, J. Tomasi, V. Barone, B. Mennucci, M. Cossi, G. Scalmani, N. Rega, G. A. Petersson, H. Nakatsuji, M. Hada, M. Ehara, K. Toyota, R. Fukuda, J. Hasegawa, M. Ishida, T. Nakajima, Y. Honda, O. Kitao, H. Nakai, M. Klene, X. Li, J. E. Knox, H. P. Hratchian, J. B. Cross, V. Bakken, C. Adamo, J. Jaramillo, R. Gomperts, R. E. Stratmann, O. Yazyev, A. J. Austin, R. Cammi, C. Pomelli, J. W. Ochterski, P. Y. Ayala, K. Morokuma, G. A. Voth, P. Salvador, J. J. Dannenberg, V. G. Zakrzewski, S. Dapprich, A. D. Daniels, M. C. Strain, O. Farkas, D. K. Malick, A. D. Rabuck, K. Raghavachari, J. B. Foresman, J. V. Ortiz, Q. Cui, A. G. Baboul, S. Clifford, J. Cioslowski, B. B. Stefanov, G. Liu, A. Liashenko, P. Piskorz, I. Komaromi, R. L. Martin, D. J. Fox, T. Keith, M. A. Al-Laham, C. Y. Peng, A. Nanayakkara, M. Challacombe, P. M. W. Gill, B. Johnson, W. Chen, M. W. Wong, C. Gonzalez and J. A. Pople, Gaussian 03, Revision C.02 (Gaussian, Inc., Wallingford CT, 2004).
61. K. Shin, I. L. Moudrakovski, C. I. Ratcliffe and J. A. Ripmeester, *Angew. Chem. Int. Ed.*, **56**(22), 6171 (2017).
62. Y. H. Ahn, Y. Youn, M. Cha and H. Lee, *Rsc Adv.*, **7**(20), 12359 (2017).

Supporting Information

Gas hydrate formation by allyl alcohol and CH_4: Spectroscopic and thermodynamic analysis

Ki Hun Park and Minjun Cha†

Department of Energy and Resources Engineering, Kangwon National University,
1 Kangwondaehak-gil, Chuncheon-si, Gangwon-do 24341, Korea
(*Received 25 July 2019 • accepted 12 November 2019*)

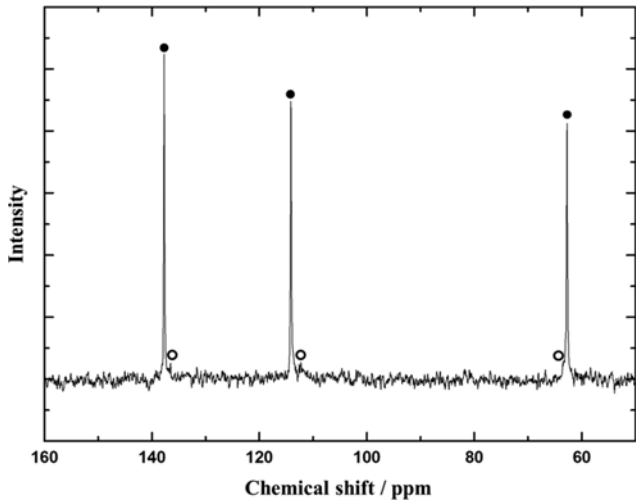

Fig. S1. Enlarged NMR spectra for the binary (allyl alcohol+methane) hydrate.

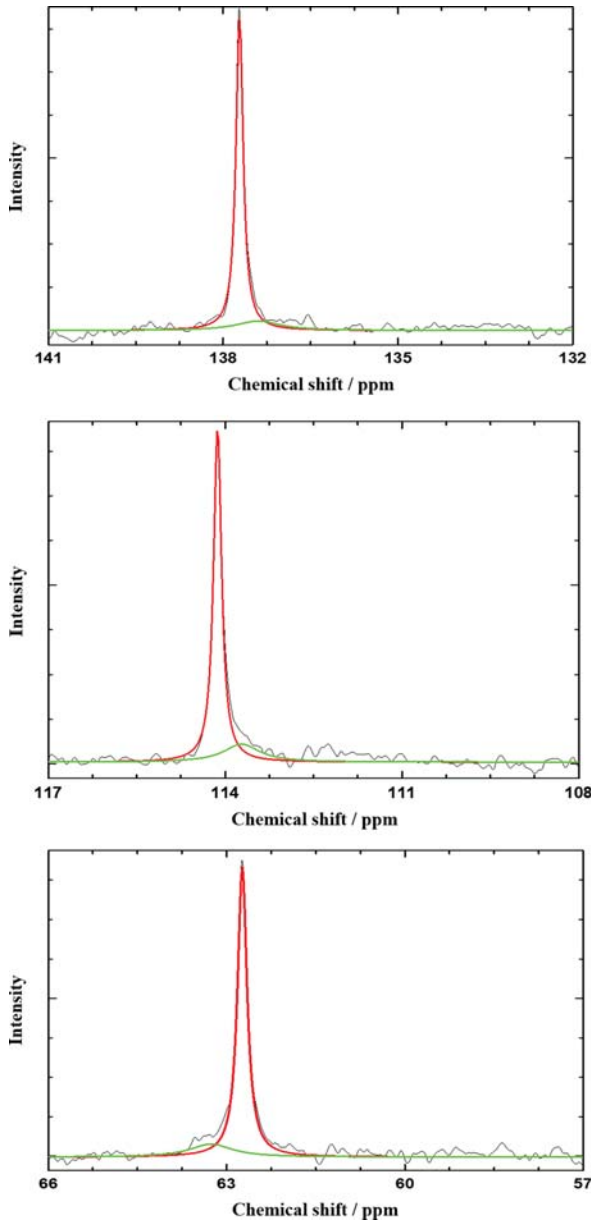

Fig. S2. Deconvoluted NMR patterns of the binary (allyl alcohol+methane) hydrate for allyl alcohol regions (Frozen allyl alcohol, red; captured allyl alcohol, light green).